A Combinatorial In Vitro/In Silico Strategy to Assess Shear-force Dependent Uptake of Nanoparticles in Vascular Microfluidic Models

Verena Charwat,[£,‡] Isabel Olmos Calvo,[†,‡] Mario Rothbauer,[¥,‡] Sebastian Rudi Adam Kratz,[¥] Christian Jungreuthmayer,[§,ℸ] Jürgen Zanghellini,[§,£] Johannes Grillari[£], and Peter Ertl[¥*]

[†]Department of Medicine III, Medical University Vienna, Austria

[£] Department of Biotechnology, University of Natural Resources and Life Sciences, Vienna, Austria

[§] ACIB - Austrian Centre for Industrial Biotechnology, Vienna, Austria

[¥] Institute of Applied Synthetic Chemistry, Institute of Chemical Technologies and Analytics, Faculty of Technical Chemistry, Vienna University of Technology, Vienna, Austria

KEYWORDS. microfluidics, in vitro, in silico, nanoparticle uptake, critical shear stress, endothelial cells

ABSTRACT: In the present work, we introduce a combinatorial approach to assess critical shear stress as a key parameter to describe and estimate nanomaterial uptake within vascular microfluidic *in vitro* models such as microchannels and perfused microsystems. We demonstrate that our complementary *in vitro*/*in silico* approach is highly suited to determine the critical flow rate above which clathrin-mediated nanoparticle uptake per cell decreases drastically even when higher nanoparticle concentrations per cell were supplied. The presented method enables more efficient testing of nanomaterial and nanomedical products since critical shear stress can be simulated as parameter for the assessment of nanomaterial uptake prior time-consuming experimental *in vitro* procedures.

The vascular system is one of the essential organ systems of the human body. Driven by the heart's pumping motion, blood is moved through the entire body via a complex vessel network to transport oxygen, nutrients, signaling molecules, carbon dioxide, waste products and many more. The continuous motion of the blood creates fluid mechanical forces, which play important roles in physiological and pathological events. Among these forces, shear stress has been identified as a main influence factor for vascular cells and tissue functions [1]. Endothelial cells, which form the inner lining of blood vessels, are highly sensitive to hemodynamic shear stresses and their phenotype (e.g. morphology, cytoskeletal structure, surface marker expression) and function (e.g. permeability and secretion of vaso-active mediators) are fundamentally altered in response to mechanical stimulation[2,3]. As wall shear stress depends in addition to flow velocities on the local vascular geometry including vessel diameter and bifurcations (e.g. branching), its magnitude varies greatly in different parts throughout the human body. Although deviating numbers are found in literature, the range of physiological shear forces starts at about 2-5 dyn/cm^{-2} in the post-capillary venules, reaches about 20-30 dyn/cm^{-2} in arteries and values up to 90 dyn/cm^{-2} are reported for smallest capillaries [4,5] [6,7]. Taking into consideration the importance of fluid mechanical forces on endothelial function, vascular researchers have already implemented a variety of perfused cell culture systems to study endothelial cell function and dysfunction including hypertension[8], platelet adhesion[9,10], angiogenesis[11], cancer extravasation[12]. Additionally, microfluidic devices containing vascular endothelial cells are increasingly being employed in biocompatibility studies, drug testing and cytotoxicity tests.[13-19] Among these cytotoxicity testing under physiological relevant measurement conditions is of particular importance in drug development efforts, since the vasculature plays a key role in uptake and distribution of drugs, toxins and nanomaterials. A special topic of increasing relevance is concerned with nanoparticle - cell interactions, due to the increased production and widespread application of engineered nanomaterials in various industries including food packaging, cosmetics, functional clothing, building industry and the medical field.[20-23] In recent years, substantial progress has also been made in the field of nanomedicine to deliver nanodrugs and contrast agents with tailor-made features such as size, shape, material and functionality including stability, magnetic and electric properties, surface functionalization, responsive materials and encapsulation.[24,25] Independent of the nanomaterial used, known features that influence cellular uptake, distribution and cytotoxicity include size, size variation, agglomeration state, number of particles, surface roughness and reactivity.[26,27] Although microfluidic cell culture systems have already been employed to assess dose-response relationships and nanomaterial-cell interactions,[22,28-34] little is still known about the influence of flow velocities and elevated shear force conditions on nanoparticle uptake rates of mammalian cells.[35,36] This aspect however is key in understanding distribution, clearance and bioaccumulation of nanomaterials in different parts of the human circulatory system. Here, we present a combinatorial approach based on experimental *in vitro* data combined with a two-step *in silico* approach based

on CFD simulations of the experimental system to identify the critical shear stress for the interaction of nanoparticles with vascular endothelial cells as a primitive model for the human vascular system.

Figure 1A shows the overall workflow for microfluidic *in* vitro experiments assessing perfused nanoparticle uptake of human endothelial cells. The general experimental setup and microfluidic design can be seen in Figure S1. As indicated earlier, shear force das a tremendous effect on endothelial phenotype and basic cellular function and morphology. Therefore, endothelial cell cultures were initially subjected to increasing flow rates thus shear up to 6.66 dyn cm^{-2} to assess the best on-chip culture protocol for 16 h prior nanoparticle exposure. Figure S2 shows that endothelial cells displayed cobblestone morphology at low shear. Relevant in vivo-like morphology was observed at shear forces above while cell elongation was induced at flow rates above 1.4 dyn cm^{-2} with even more pronounced morphological changes and cell elongation along the trajectory after an exposure period of 12 h at shear force conditions between above 3 dyn cm^{-2} (e.g. 6.66 dyn cm^{-2}). Based on these results, a 16 h pre-incubation period at a shear of approx. 3 dyn cm^{-2} was employed prior nanoparticle uptake experiments to render endothelial cultures more *in vivo*-like. A biocompatibility study in the presence of increasing concentrations of fluorescent polystyrene nanoparticles revealed no detrimental effects on metabolic activity of endothelial cells with values of 0.83 ± 0.08 and 0.88 ± 0.11 for 49 nm and 249 nm polystyrene nanoparticles at a concentration of 4 %, respectively. Figure 1BC shows nanoparticle uptake under standard static cell culture conditions to assess intracellular uptake and accumulation at increasing concentrations of 0.1, 1, 4 and 10 % nanoparticle solutions (0.01, 0.1, 0.4 and 1 mg mL^{-1}, respectively) for up to 24 h. In contrast to plate reader readout (data not shown), flow cytometry and image analysis provided results with low background noise as only the cells, but not the underlying polymer substrate contributed to the signal. Time and dose dependency of uptake curves was observed for both polystyrene nanoparticle types. Fluorescent signals displayed a slight decrease in uptake after 12 h incubation time for 249 nm nanoparticles interestingly at concentrations above 4%. For smaller nanoparticles, cellular uptake under static conditions displayed linear behavior for both, time- as well as concentration dependency. Figure 1D shows the impact of perfused nanoparticle uptake scenarios on endothelial cells. Static exposure scenarios revealed areas of low fluorescence intensity (top panel, white arrow) around individual cells, which was completely impeded for perfused culture conditions. In a static scenario, nanomaterial uptake results in depletion areas at the cell vicinity with particle aggregation predominantly around the nucleus, whereas perfused nanomaterial exposure without sedimentation displays more homogenously distributed nanoparticle uptake void from depletion areas (bottom panel).

To distinguish between nanoparticle adhesion on the cellular membrane and actual uptake, confocal microscopy was performed as depicted in Figure 2. Figure 2A shows confocal images of endothelial cells incubated with 249 nm nanoparticles displaying localization of nanoparticles in the cytoplasm around the nucleus. Especially for confluent cell populations, endocytosis mainly occurs through the clathrin-mediated pathway.[37]

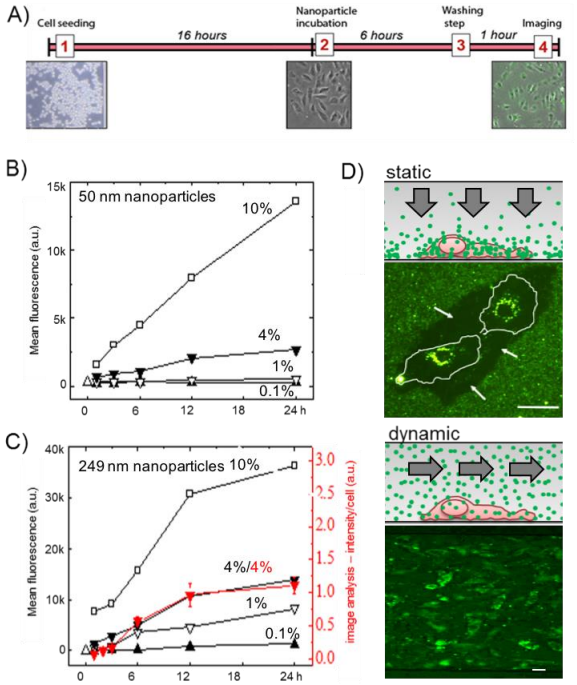

Figure 1. (A) Workflow of the experimental microfluidic protocol for assessment of critical shear force on endothelial microvascular models. (B, C) Quantification of time and dose dependent uptake of 49 nm (B) and 249 nm (C) polystyrene nanoparticles using flow cytometry. Complementary data analysis derived from image analysis *in situ* is shown for 4% 249 nm polystyrene nanoparticles (red curve). (D) Fluorescence images of HUVEC incubated with 4% 249 nm nanoparticles overnight under static and dynamic conditions. In the static fluorescence image cell outlines are marked in white and arrows indicate the NP-depleted area around the cells. Scale bars, 50 µm.

Therefore, flow cytometric analysis was performed to determine cellular uptake routes and to distinguish between active and passive uptake pathways. In a next set of experiments, endothelial cell cultures were incubated with 4% NP suspensions for 6 h using static cultivation conditions. Exposure to saccharose was used to inhibit clathrin-mediated pathways and incubation at 4 °C blocked any active uptake routes, both effective inhibition strategies as reported in literature.[38] Figures 2C shows that both 49 nm NPs and 249 nm nanoparticles faced active uptake mechanisms, since intracellular uptake was considerably reduced at low temperature. Inhibition of clathrin-dependent endocytosis by incubation with saccharose further confirmed the involvement of active uptake via clathrin-dependent routes for both nanoparticle sizes. An increase of concentration of saccharose from 0.12 M to 0.45 M reduced cellular uptake of the 249 nm nanoparticles from about 90% to 5%. In other words, 249 nm polystyrene nanoparticles are almost exclusively actively transferred into the cell via clathrin-mediated pathway, while approx. 25% of the 49 nm nanoparticles cross the cell membrane passively due to the small diameter. Based on these results, uptake of 249 nm nanoparticles was chosen for subsequent measurements to eliminate passive transport and focus on active, clathrin-dependent nanomaterial uptake for the presented *in vitro/in silico* approach.

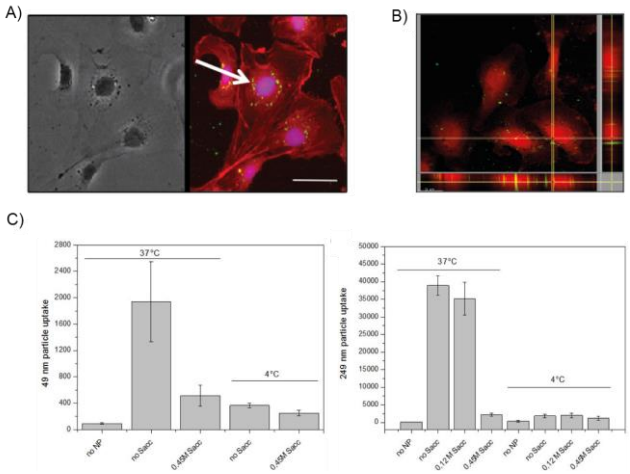

Figure 2. (A) Interference and fluorescence microscopy overlay of blue (nucleus), red (f-actin) and green (249 nm nanoparticles) show localization in the cytoplasm around the nuclei. Scale bar, 50 µm. (B) Top view and cross sections of a z-stack (plane resolution 2 µm) showing cell cytoplasm (red) and 249 nm nanoparticles (green). (C) Identification of passive uptake and clathrin-dependent endocytosis as the uptake mechanism for 50 nm and 249 nm nanoparticles. To inhibit active uptake samples were exposed to low temperature (4ºC) and saccharose.

Figure 3 shows proof of principle experiments of uptake analysis of 249 nm nanoparticles using the proposed combinatorial *in vitro/in silico* analysis approach for assessment of critical shear force. Initially, after 16 h of microfluidic culture of confluent endothelial cell populations, microfluidic uptake experiments of 249 nm nanoparticles at a concentration of 4% were performed over a total period of 6 h. Figure 3A (top panel) shows results of the microfluidic experiments in the presence of 0, 0.045, 0.225, 0.45, 2.25, 3.6, 4.5 and 9 µL min^{-1} with corresponding to calculated wall shear stress values of 0, 0.1, 0.5, 1, 5, 8, 10 and 20 dyn cm^{-2}, respectively. Below a flow rate of 2.25 µL min^{-1} (4 dyn cm^{-2}) gradual increase of nanoparticles was observable. Interestingly, above that shear stress, nanoparticle uptake gradually decreased. For example, an increase of flow rate from 2.5 to 4.5 µL min^{-1} resulted in a 70% decrease of nanoparticles taken up by endothelial cells. To rule out that the gradual increase of clathrin-mediated nanoparticle uptake below the shear threshold is caused not by shear stress and shear-dependent changes in cell surface levels of clathrin, but simply increasing numbers of nanoparticles on the cell surface, in a next set of experiments endothelial cells were subjected to gradually increasing flow rates thus shear stress for 6 h. Figure S-5A shows a light increase of clathrin receptors on the cell surface by 1,27-fold and 1,74-fold for endothelial cells subjected to shear of 1.69 dyn cm^{-2} and 3.5 dyn cm^{-2}.

Figure S-5B shows that for the same number of nanoparticles transported to the cell surface during 6 h of exposure at shear below the threshold, the nanoparticle solution at 4% resulted in 2,8-fold more uptake of 249 nm polystyrene nanoparticles than the 2% solution. These results indicate that below the shear threshold,

Figure 3A (bottom panel) shows two *in silico* approaches for determination of wall shear force either using a simplified a parallel plate model (analytical, red curve; see also Figure S3A) or more complex CFD model (green curve; see also Figure S3BC). The decrease of particle uptake above 2.25 µL min^{-1} with linear increase of wall shear stress suggests that above a critical shear stress the interaction time between nanoparticles and the cell surface becomes insufficient, thus severely limiting the probability of uptake via clathrin-dependent endocytosis. Because it is well known that ligand-receptor interactions at the cell surface require sufficient interaction time due to the probabilistic nature of receptor-ligand bond formation under fluid shear force [39,40], we hypothesize that similar effects take place during nanoparticle adhesion at the cell membrane and cellular uptake. Figure 3B shows again, both, an analytical as well as a CFD in silico approach to determine total mass of particles touching the cell surface at different flow rates (see Equations S2 to S4). Results of the flow rate dependent adherent particle mass are plotted in Figure 3B (red curve) with a critical shear stress of τ_{crit} = 0.170 Pa (G_{crit} = 242.86 s^{-1}). Even though robust and simple, the analytical approach cannot account for complex biological parameters such as cell shape, surface charge, cell deformability as well as particle trajectories. Therefore, the more accurate CFD approach was used to estimate nanoparticle movement (see Figure S4), adhesion and escape and numerous physical parameters including pressure, fluid velocity, wall shear stress and kinetic energy which were calculated at each mesh point of the geometric model. Nanoparticle movement was simulated by *Starccm+*'s Lagrangian particle tracking model, where trajectories of 57 000 particles moving through the microchannel were computed (see Figure S4A). Figure 3B revealed a maximum particle escape rate of 1871 particles escaping per second for a simulated input flow rate of 0.045 µL min^{-1} (blue curve). While higher input flow rates resulted in a lower number of escaped particles, theoretical adhered particle mass increased linear with the input flow rate (green curve). Finally, the experimental *in vitro* data was fitted into a flow-dependent NP uptake function (see Equation S7). The calculated critical shear stress was τ_{crit} of 0.179 dyn cm^{-2} (G_{crit} = 255.71 s^{-1}) and τ_{crit} = 0.170 dyn cm^{-2} (G_{crit} = 242.86 s^{-1}) for analytical and CFD simulations, respectively. Figure 3C shows that both *in silico* approaches correspond very well with experimental *in vitro* data. Despite the good concordance of the simulated critical shear force values with experimental data, the employed CFD simulation, however, enables the control of even more experimental parameters such as cell morphology, cell elasticity, nanoparticle size, nanoparticle density, nanoparticle charge, etc.

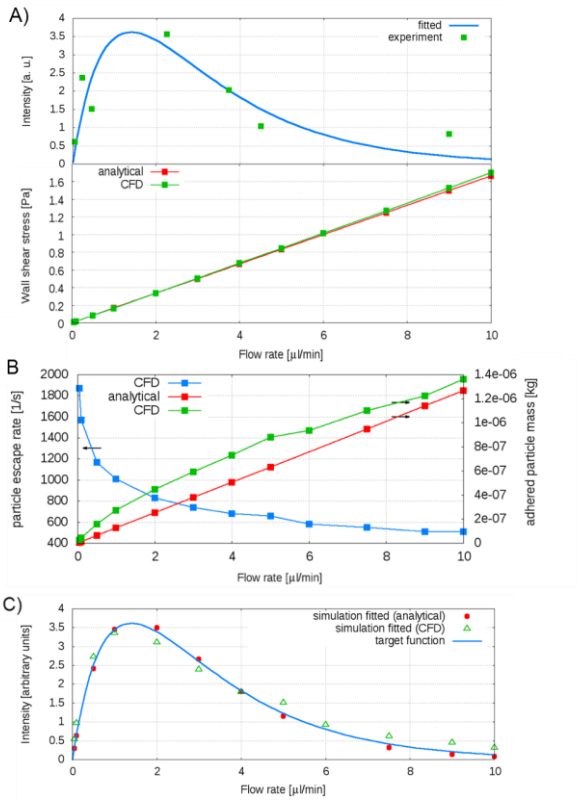

Figure 3. (A) Flow rate dependent uptake of 249 nm nanoparticles by endothelial cells using the combinatorial method based on experimental results (green squares, top panel) and a mathematical fitting function (blue curve, top panel), as well as the position-independent wall shear stress (bottom panel, red curve) and the critical wall shear stress (bottom panel, blue curve) as a function of input flow rate. (B) Rate of particles escaping the simulation volume via cell surfaces as function of the input flow rate (blue line, left y-axis) with mass of adhered nanoparticles on the cell surface. (red and green lines, right y-axis). (C) Combinatorial approach to identify critical shear stress parameters obtained by experimental *in vitro* (fitted blue line) and in silico CFD approaches (red and green symbols).

The combinatorial method in vitro/in silico method presented here is straightforward and offers the possibility to screen for nanomaterial uptake by assessment of critical shear force as parameter heavily influencing nanomaterial-cell surface interaction within dynamic biological model systems. This will greatly facilitate to assess the impact of critical nanomaterial parameters (e.g. geometry, surface chemistry, surface roughness, density, etc.) during the design of novel nanomaterials since computational methods that enable prediction of experimental data are easily up-scalable, and provide high-content and –throughput data prior time- and cost-intensive actual experimental screening.

ASSOCIATED CONTENT

Supporting Information

The Supporting Information is available free of charge on the ACS Publications website. Additional figures as noted in the manuscript text, simulation details, experiment details (.pdf).

AUTHOR INFORMATION

Corresponding Author

* peter.ertl@tuwien.ac.at

Present Addresses

ⵊ current address: Department of Biomedical and Health Technologies, Vienna, Austria

Author Contributions

The manuscript was written through contributions of all authors. / All authors have given approval to the final version of the manuscript. / ‡These authors contributed equally.

ACKNOWLEDGMENT

(Word Style "TD_Acknowledgments"). Generally the last paragraph of the paper is the place to acknowledge people (dedications), places, and financing (you may state grant numbers and sponsors here). Follow the journal's guidelines on what to include in the Acknowledgement section.

REFERENCES

(1) Paszkowiak, J. J.; Dardik, A. *Vascular and endovascular surgery* **2003**, *37*, 47-57.

(2) Davies, P. F. *Nature clinical practice Cardiovascular medicine* **2009**, *6*, 16-26.

(3) Reneman, R. S.; Arts, T.; Hoeks, A. P. *Journal of vascular research* **2006**, *43*, 251-269.

(4) Koutsiaris, A. G.; Tachmitzi, S. V.; Batis, N.; Kotoula, M. G.; Karabatsas, C. H.; Tsironi, E.; Chatzoulis, D. Z. *Biorheology* **2006**, *44*, 375-386.

(5) McNicol, G.; Lowe, G.; Barbenel, J.; Forbes, C. *Clinical aspects of blood viscosity and cell deformability*; Springer Science & Business Media, 2012.

(6) Osinnski, J. N.; Ku, D. N.; Mukundan, S.; Loth, F.; Pettigrew, R. I. *Journal of Magnetic Resonance Imaging* **1995**, *5*, 640-647.

(7) Oyre, S.; Pedersen, E. M.; Ringgaard, S.; Boesiger, P.; Paaske, W. *European journal of vascular and endovascular surgery* **1997**, *13*, 263-271.

(8) Hu, R.; Li, F.; Lv, J.; He, Y.; Lu, D.; Yamada, T.; Ono, N. *Biomed Microdevices* **2015**, *17*, 1-9.

(9) Conant, C. G.; Schwartz, M. A.; Nevill, T.; Ionescu-Zanetti, C. *Journal of visualized experiments: JoVE* **2009**.

(10) Ku, C.-J.; D'Amico Oblak, T.; Spence, D. M. *Analytical chemistry* **2008**, *80*, 7543-7548.

(11) Chung, S.; Sudo, R.; Vickerman, V.; Zervantonakis, I. K.; Kamm, R. D. *Annals of biomedical engineering* **2010**, *38*, 1164-1177.

(12) Jeon, J. S.; Zervantonakis, I. K.; Chung, S.; Kamm, R. D.; Charest, J. L. *PloS one* **2013**, *8*, e56910.

(13) Jeong, G. S.; Kwon, G. H.; Kang, A. R.; Jung, B. Y.; Park, Y.; Chung, S.; Lee, S.-H. *Biomed Microdevices* **2011**, *13*, 717-723.

(14) Dereli-Korkut, Z.; Akaydin, H. D.; Ahmed, A. R.; Jiang, X.; Wang, S. *Analytical chemistry* **2014**, *86*, 2997-3004.

(15) Lee, H.; Kim, S.; Chung, M.; Kim, J. H.; Jeon, N. L. *Microvascular research* **2014**, *91*, 90-98.

(16) Sticker, D.; Lechner, S.; Jungreuthmayer, C.; Zanghellini, J.; Ertl, P. *Anal Chem* **2017**, *89*, 2326-2333.

(17) Rothbauer, M.; Zirath, H.; Ertl, P. *Lab on a Chip* **2017**.

(18) Rothbauer, M.; Wartmann, D.; Charwat, V.; Ertl, P. *Biotechnol Adv* **2015**, *33*, 948-961.

(19) Ertl, P.; Sticker, D.; Charwat, V.; Kasper, C.; Lepperdinger, G. *Trends Biotechnol* **2014**, *32*, 245-253.

(20) Savolainen, K.; Backman, U.; Brouwer, D.; Fadeel, B.; Fernandes, T.; Kuhlbusch, T.; Landsiedel, R.; Lynch, I.; Pylkkänen, L. *Helsinki, Finnish Institute of Occupational Health* **2013**.

(21) Gaspar, R. **2007**.

(22) Mahto, S. K.; Charwat, V.; Ertl, P.; Rothen-Rutishauser, B.; Rhee, S. W.; Sznitman, J. *Nanotoxicology* **2014**, 1-15.

(23) Netzer, K.; Jordakieva, G.; Girard, A. M.; Budinsky, A. C.; Pilger, A.; Richter, L.; Kataeva, N.; Schotter, J.; Godnic-Cvar, J.; Ertl, P. *Basic Clin Pharmacol Toxicol* **2017**.

(24) Juliano, R. *Nature Reviews Drug Discovery* **2013**, *12*, 171-172.

(25) Rizzo, L. Y.; Theek, B.; Storm, G.; Kiessling, F.; Lammers, T. *Current opinion in Biotechnology* **2013**, *24*, 1159-1166.

(26) Soenen, S. J.; Rivera-Gil, P.; Montenegro, J.-M.; Parak, W. J.; De Smedt, S. C.; Braeckmans, K. *Nano Today* **2011**, *6*, 446-465.

(27) De Jong, W. H.; Borm, P. J. *Int J Nanomed* **2008**, *3*, 133.

(28) Mahto, S. K.; Yoon, T. H.; Rhee, S. W. *Biomicrofluidics* **2010**, *4*, 034111.

(29) Richter, L.; Charwat, V.; Jungreuthmayer, C.; Bellutti, F.; Brueckl, H.; Ertl, P. *Lab on a Chip* **2011**, *11*, 2551-2560.

(30) Sticker, D.; Rothbauer, M.; Lechner, S.; Hehenberger, M. T.; Ertl, P. *Lab Chip* **2015**, *15*, 4542-4554.

(31) Charwat, V.; Rothbauer, M.; Tedde, S. F.; Hayden, O.; Bosch, J. J.; Muellner, P.; Hainberger, R.; Ertl, P. *Anal Chem* **2013**, *85*, 11471-11478.

(32) Shoshi, A.; Schotter, J.; Schroeder, P.; Milnera, M.; Ertl, P.; Heer, R.; Reiss, G.; Brueckl, H. *Biosens Bioelectron* **2013**, *40*, 82-88.

(33) Charwat, V.; Joksch, M.; Sticker, D.; Purtscher, M.; Rothbauer, M.; Ertl, P. *Analyst* **2014**, *139*, 5271-5282.

(34) Rothbauer, M.; Frauenlob, M.; Gutkas, K.; Fischer, M. B.; Sinner, E. K.; Kupcu, S.; Ertl, P. *ACS Appl Mater Interfaces* **2017**, *9*, 34423-34434.

(35) Moghimi, S. M.; Hunter, A.; Andresen, T. *Annual review of pharmacology and toxicology* **2012**, *52*, 481-503.

(36) Rothbauer, M.; Praisler, I.; Docter, D.; Stauber, R. H.; Ertl, P. *Biosensors (Basel)* **2015**, *5*, 736-749.

(37) Snijder, B.; Sacher, R.; Ramo, P.; Damm, E. M.; Liberali, P.; Pelkmans, L. *Nature* **2009**, *461*, 520-523.

(38) Silverstein, S. C.; Steinman, R. M.; Cohn, Z. A. *Annu Rev Biochem* **1977**, *46*, 669-722.

(39) Cozensroberts, C.; Lauffenburger, D. A.; Quinn, J. A. *Biophys J* **1990**, *58*, 841-856.

(40) Hammer, D. A.; Lauffenburger, D. A. *Cell Biophys* **1989**, *14*, 139-173.

ToC

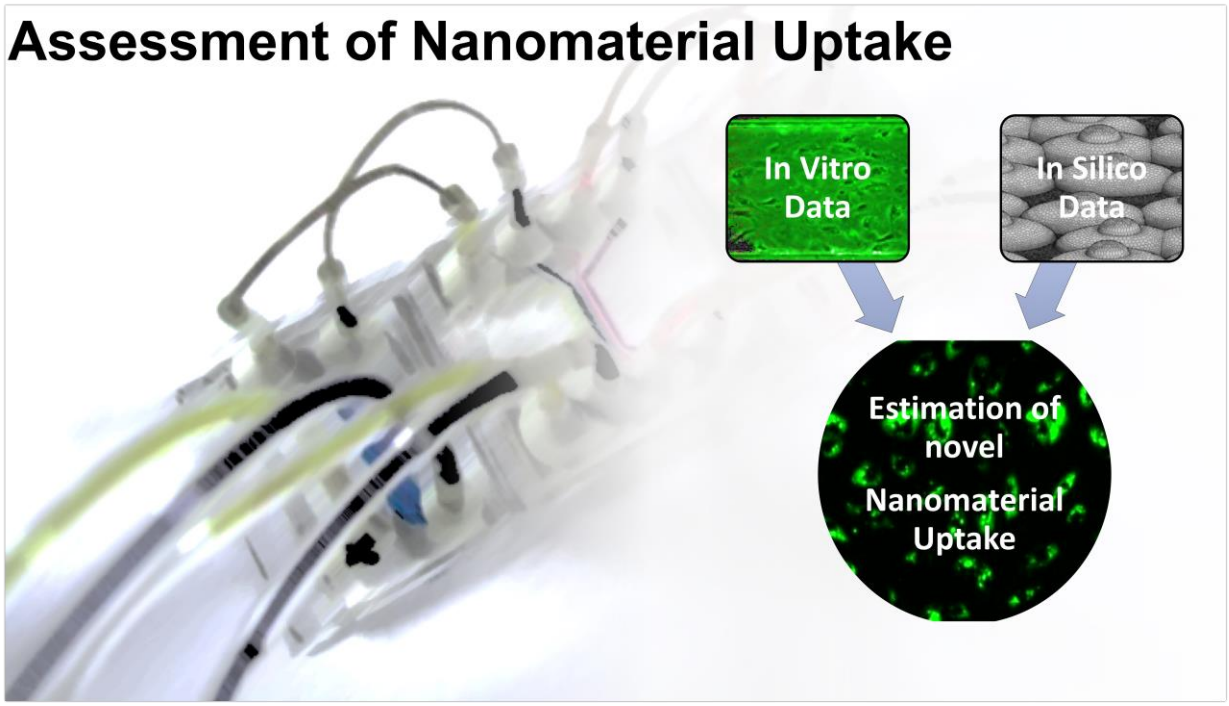
Assessment of Nanomaterial Uptake
In Vitro Data
In Silico Data
Estimation of novel Nanomaterial Uptake